

# The Wilberforce pendulum: a complete analysis using micro accelerometer/gyroscope, smartphone and dynamical modeling



Giacomo Torzo<sup>1</sup>, Massimiliano Zanichelli<sup>2</sup>, Stefano Pasqualotto<sup>3</sup>, Michele D'Anna<sup>4</sup>

<sup>1</sup> AIF and Dept. of Physics, Padova University, via Marzolo 8, Padova, Italy

<sup>2</sup> IISS Emilio Gadda, via Nazionale 6, Fornovo, Italy

<sup>3</sup> LabTrek, via B. Cristofori 31, Padova, Italy

<sup>4</sup> Liceo cantonale, Locarno, Switzerland (retired)

ISSN 1870-9095

E-mail: torzog@gmail.com

(Received 27 November 2024, accepted 15 February 2025.)

## Abstract

The Wilberforce pendulum is a didactical device often used in class demonstrations to show the amazing phenomenon of coupled oscillations (rotational and longitudinal) producing beats in a special mass-spring set up. The phenomenon is particularly surprising for a distant observer, who easily detects the longitudinal motion, but may skip the presence of rotation. To him (her) the vertical oscillation appears to damp out completely and then it rises again without external action (as if an invisible force would come in). In this paper we propose a revised version of the classical experiment, suggesting a deeper understanding of phenomena through real time data acquisition of both the rotation and the vertical oscillation, using a MEMS accelerometer/gyroscope and the free software Phyphox to show the device motion on a smartphone screen. A detailed analysis of the motion and of the energetical aspects are then performed using the free modeling tool InsightMaker.

**Keywords:** Wilberforce pendulum, Data handling and computation, Accelerometer, Gyroscope, Phyphox, Dynamical modeling

**PACS:** 06.50, 07.10, 46.30P, 02.60.Cb, 07.05.Tp

## I. INTRODUCTION

The Wilberforce pendulum [1] picked up the curiosity of many authors [2,3,4,5,6], among which Arnold Sommerfeld, who wrote a complete theoretical treatment [7,8,9]. Recently it was studied also using either real-time data acquisition systems (sonar interfaced to a PC by measuring only the vertical oscillation) [10], video camera and complex software/hardware [11], or accelerometer/gyroscope [12] (but using expensive dataloggers and software), or using accelerometer/gyroscope integrated in smartphones (however missing a complete record of rotational and longitudinal motions) [13,14,15].

Commercial Wilberforce pendulums are also available, with *indirect* measurements of the  $z$  vertical displacement and the  $\alpha$  rotation angle, using torque/force sensor, which require expensive dataloggers and software [16].

Here we report experimental results obtained with a *wireless* device that characterizes the Wilberforce pendulum motion both for vertical and rotational oscillations, requiring nor datalogger, nor software, but simply a common smartphone or tablet.

## II. THE EXPERIMENTAL SETUP

The Wilberforce pendulum dynamic includes three different kinds of motion: two roto-translational oscillations and a mixed oscillation with beatings, in which the energy of the system is transferred between the vertical and rotational oscillations. This peculiar behavior is obtained if:

- rigid connections are provided at both ends of the helicoidal right-hand spring,
- the ratio  $k/\delta$  between the longitudinal elastic constant  $k$  and the torsional elastic constant  $\delta$  does closely match the ratio  $m/I$  between the mass  $m$  and the inertial moment  $I$ .

Our pendulum (figure 1) uses a 50 turns stainless steel spring (25 mm coil diameter, 1.3 mm wire diameter) and a brass cylindrical bob of about 0.5 kg (with 4 screws for fine-tuning of the inertial moment), and at the bottom a MEMS absolute orientation sensor (including accelerometer and gyroscope) driven by an ESP32 microcontroller with built-in WIFI and Bluetooth and Li-ion battery charger

The top end of the spring is fixed to a brass cylinder that may both rotate along the vertical axis and shift in vertical direction (figure 2).

By a proper choice of initial displacement  $z_0$  and rotation angle  $\alpha_0$  we may excite each one of the three different pendulum motions we are interested in.

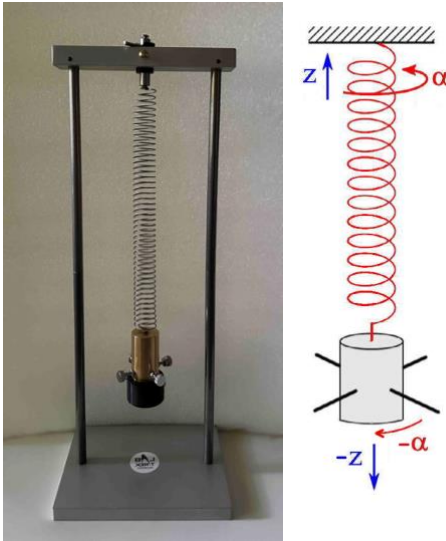


FIGURE 1. The Wilberforce pendulum.

The mechanical device shown in figure 2 works as follows: a small manual clockwise rotation of the horizontal bar gives to the upper end of the spring both an upward shift and a clockwise rotation (due to the inclines of the hollow cylinder top). Note that that an action applied to the upper end of the spring corresponds to an opposite action applied to the bob: in this case a bob displacement  $z_0 < 0$  and a bob rotation  $\alpha_0 < 0$  (normal mode 1, with  $z_0$  and  $\alpha_0$  in phase, see section V). A rotation of the bar in the opposite direction excites the normal mode 2 (with  $z_0$  and  $\alpha_0$  in phase opposition).



FIGURE 2. Roto-translational suspension device.

The boards with the MEMS sensor, the microprocessor and the battery are inserted into a 3D-printed enclosure that is screwed at the brass cylinder bottom.

Using Arduino programmer, we uploaded to the ESP32 code for Bluetooth connection to the Phyphox application, and for a simple data conversion of the MEMS sensor output signals (vertical acceleration  $a_z$  and rotation angle  $\alpha$ ). Knowing the values of the elastic constant  $k$  and of the oscillating mass  $m$ , using the Newton law ( $F_z = ma_z$ ), the Hooke law ( $F_z = -kz - \varepsilon\alpha$ ) (modified by the *elastic coupling term* as explained in SECTION IV), from the measured acceleration values  $a$  we calculate the displacement values  $z$  through the equation:

$$z = - (m/k)a + (\varepsilon/k)\alpha/2 \quad (1)$$

### III. EXPERIMENTAL RESULTS

An example of the recorded rotation angle and of the vertical displacement is shown in figure 3, where the beats are evident: the vertical oscillation slowly dumps-out while rotational oscillation rises, then the process reverses (approximately every 1/2 minute) with the energy associated to each oscillation that transfers from one motion to the other, with small dissipation.

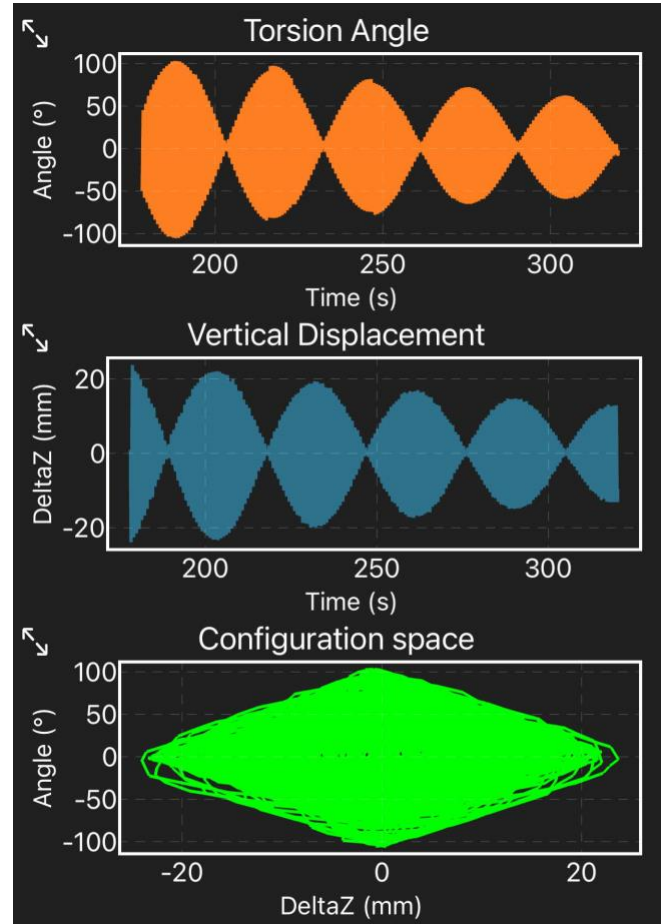


FIGURE 3. Example of data recorded for mixed motion. Top graph: rotation angle  $\alpha$ . Middle graph: vertical displacement  $z$ . Bottom graph: angle  $\alpha$  vs. displacement  $z$ .

In figure 3 the longitudinal and torsional oscillations excited by starting the motion with initial displacement  $z=25$  mm and  $\alpha=0$  have the same period. This condition is needed to achieve a complete energy exchange. The period matching may be obtained by adjusting the moment of inertia of the oscillating bob through the 4 screw knobs protruding from the brass cylinder.

### IV. ENERGY ANALYSIS

In order to study the time evolution of the energy of our system (both vertical and rotational oscillation) we need to consider a kinetic term  $E_k$  and an elastic potential term  $E_e$  [17]. For the *Translational* motion we have:

$$E_T = E_{kT} + E_{eT} = mv^2/2 + kz^2/2 \quad (2)$$

where  $m$  is the mass of the oscillating bob,  $v$  its velocity,  $k$  the elastic constant of the spring, and  $z$  its vertical displacement from the equilibrium position. For the *Rotational* motion we have:

$$E_R = E_{kR} + E_{eR} = I\omega^2/2 + \delta\alpha^2/2 \quad (3)$$

where  $I$  is the moment of inertia of the bob,  $\omega = d\alpha/dt$  its angular velocity,  $\delta$  the torsional constant of the spring and  $\alpha$  the rotation angle.

We note that in order to obtain a complete expression of the *total energy* of the system, it is not necessary to describe the damping explicitly (since the dynamic values update their respective energy contributions at each instant). However, in addition to the four contributions above, it is *necessary* to introduce a term describing the interaction between translation and rotational motion. Following the model proposed by Sommerfeld [7], we introduce the *coupling energy*  $E_c = \varepsilon\alpha z/2$ , where  $\varepsilon$  is the *coupling coefficient* which characterizes the spring and depends on its geometric properties as well as on the mechanical properties of the material of which the spring is made. The complete equation for the Wilberforce pendulum energy is therefore:

$$E_{Wilber} = E_T + E_R + E_c = (mv^2 + kz^2 + I\omega^2 + \delta\alpha^2 + \varepsilon\alpha z)/2 \quad (4)$$

In order to evaluate the behavior of the various terms one must know the values of the four parameters  $m$ ,  $k$ ,  $I$  and  $\delta$ .

To determine  $k$  we may measure the spring elongation under a known force (e.g. the cylinder weight  $mg$ ).

A measurement of the moment of inertia  $I$  for our *non-cylindrical* bob (consisting of the brass cylinder, its protruding screws, and the box containing the electronics attached at the bottom) may be obtained through two measurements of the rotational period: first with the bob only, and then by adding an *annular cylinder* (of known mass  $M$ , inner radius  $R_i$ , outer radius  $R_o$ ), whose moment of inertia is  $I_a = M(R_o^2 + R_i^2)/2$ .

The two periods (without and with the annular cylinder) obey to the relations:  $(T/2\pi)^2 = I_x/\delta$ ,  $(T_1/2\pi)^2 = (I_x + I_a)/\delta$ , giving:  $I_x = I_a T^2 / (T_1^2 - T^2)$ .

We can finally determine the *torsion constant*  $\delta$  from the measured period  $T = 2\pi/\omega$ :  $\delta = I(2\pi/T)^2$ .

## V. NORMAL MODES

To find out the frequencies of the normal modes of the Wilberforce pendulum, we begin by analyzing the vertical displacement  $z(t)$  in the case where there are beats that totally transfer energy from translational to rotational motion (Figure 3). The initial conditions for achieving this situation are met by displacing the pendulum bob vertically by  $z(0) = z_0$ , with no rotation ( $\alpha(0) = 0$ ) and releasing it from rest ( $v(0) = 0$  and  $\omega(0) = 0$ ).

Under these circumstances the Fast Fourier Transform (FFT) of the data illustrated in Figure 3 for the vertical  $z$  displacement shows two distinct peaks (of the same height) at frequencies 1.26 Hz and 1.29 Hz (figure 4). This is due to the intrinsic coupling between two normal modes.

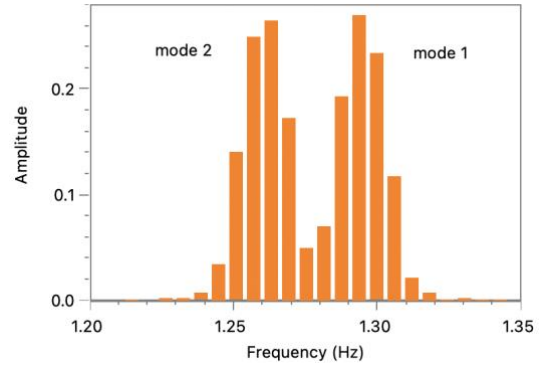


FIGURE 4. FFT of the data illustrated in Figure 3 for the vertical displacement  $z$ .

These latter can be excited by properly choosing the initial conditions, as explained in section II. The records of rotations and translations for the two normal modes, are illustrated in figure 5.

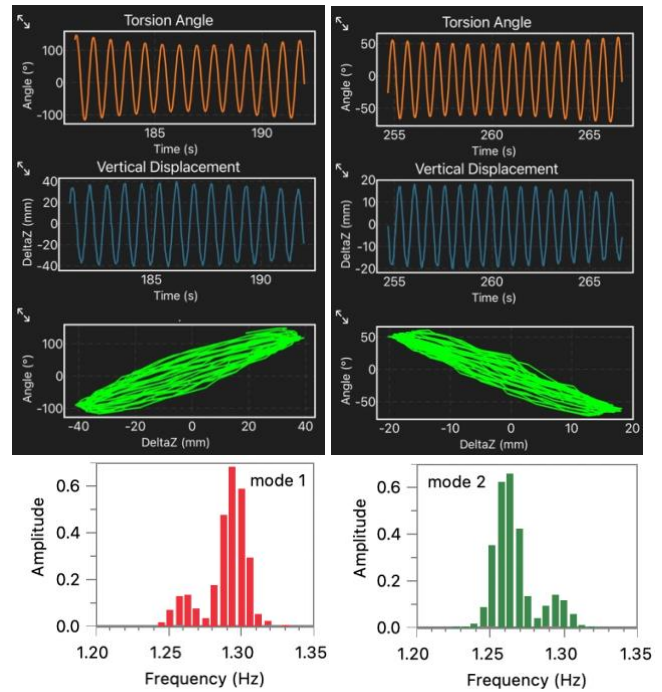


FIGURE 5. Example of data recorded for the two normal modes and corresponding FFT graphs.

The analysis of the motion equations giving the frequencies of the two normal modes  $\omega_1$  and  $\omega_2$  may be found in several papers [2 - 9]. Here we limit ourselves to the case where the pendulum is fine-tuned, a situation achieved when the vertical and rotational motions show the same frequency, i.e., when  $\omega_z = (k/m)^{1/2} = \omega_\alpha = (\delta/I)^{1/2} = \omega_0$ . In this case the beat frequency  $\omega_B$  (related to the rapidity of energy transfer) is largely smaller than the mechanical oscillation frequency. This allows us to use the linearized relations [3], which are valid precisely in the case of weak coupling, easier to handle:

$$\begin{aligned} \omega_1 &= \omega + \varepsilon/4(kI)^{1/2} \\ \omega_2 &= \omega - \varepsilon/4(kI)^{1/2} \end{aligned} \quad (5)$$

It can be demonstrated [3] that the normal modes (no beatings) can be excited by choosing initial conditions:  $z_0 = +\Gamma\alpha_0$  for the normal mode 1 and  $z_0 = -\Gamma\alpha_0$  for the normal

mode 2, where  $\Gamma = (I/m)^{1/2}$  is the *radius of gyration* of the pendulum. Then, keeping in mind the relationship expressing the interaction energy ( $E_\varepsilon = \varepsilon z \alpha / 2$ ), we can say that normal mode 1 is the one characterized by *higher energy* and *in-phase* changes of displacement and angle (with our right-hand helical spring  $z$  and  $\alpha$  have same sign), while normal mode 2 the one characterized by *lower energy* and a *phase-opposition* of displacement and angle ( $z$  and  $\alpha$  have opposite sign).

The difference  $\omega_1 - \omega_2$  is the *beating frequency*  $\omega_B$ :

$$\omega_B = \varepsilon / 2(kI)^{1/2} \quad (6)$$

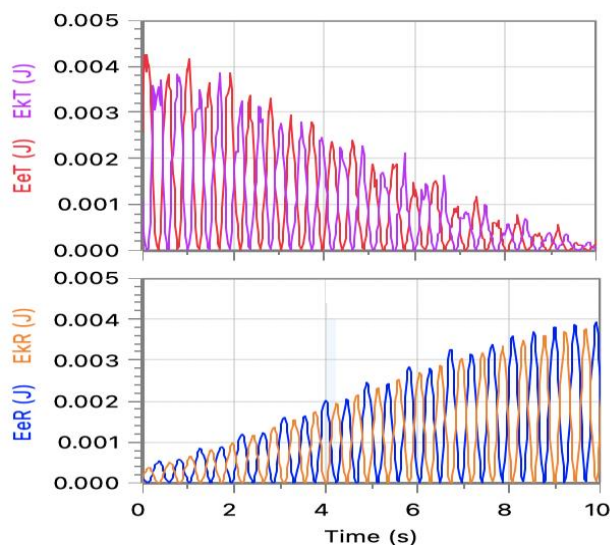
The value of the coupling constant  $\varepsilon$  determines the beating period  $T_B = 2\pi/\omega_B$ . The stronger is the coupling the faster becomes the energy transfer across modes, the shorter becomes the beating period.

A value for  $\varepsilon$  can therefore be obtained from experimental data, measuring the frequencies  $\omega_1$  and  $\omega_2$ : in fact, from equations (5) and (6) we get  $\varepsilon = 2(\omega_1 - \omega_2)(kI)^{1/2}$ .

## VI. ANALYSIS WITH EXCEL

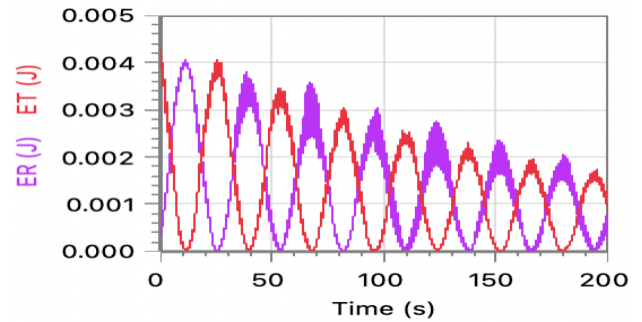
As first step we study the experimental results by using real data uploaded into an Excel® spreadsheet (data export through WIFI connection is included in *Phyphox* application). Using standard Excel tools we calculate the various energy terms.

Once we have determined the four parameters  $m$ ,  $k$ ,  $I$  and  $\delta$  we calculate the *elastic* and *kinetic* energies from the measured angles and displacements, as shown in figure 6.



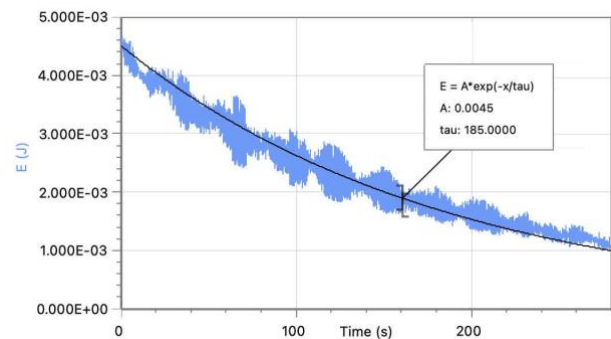
**FIGURE 6.** Elastic ( $E_e$ ) and kinetic ( $E_k$ ) energies for rotational and translational motions vs. time.

Figure 6 shows the periodic transformation of the elastic energy into kinetic energy, both for translation and rotation. The sum of kinetic energy and elastic energy for each motion, illustrated in figure 7,  $E_T = E_{eT} + E_{kT}$  and  $E_R = E_{eR} + E_{kR}$ , shows the transfer of energy from oscillation and rotation with much small frequency  $\omega_B$ .



**FIGURE 7.** Translational  $E_T$  and rotational  $E_R$  energies vs. time.

By finally adding the three terms  $E_T(t)$ ,  $E_R(t)$  and  $E_\delta(t)$  we obtain the total energy that appears to decrease very slowly in time (in figure 8 we see that the time constant in the fitting exponential decay is about 185 s). The oscillations that affect the calculated values in this graph may be attributed to “noise” in the recorded data and to the incertitude in the parameters  $m$ ,  $k$ ,  $I$ ,  $\delta$  and  $\varepsilon$ .



**FIGURE 8.** Calculated  $E_T(t) + E_R(t) + E_\delta(t)$  as function of time.

The use of Excel to obtain figures 6, 7 and 8 requires a long data handling: e.g. for translations: a *recursive formula* must be used to calculate in the first data row for each time interval  $dt$ , the variation in speed  $dv/dt$  (from the initial acceleration  $-(kz_0 + \varepsilon\alpha_0)/m$ , then the variation of  $z$  (from  $dz/dt$ ), and finally the acceleration calculated for the new  $z$  is placed in the next row (end of the cycle). Then, by *click-dragging* in each column, the data are calculated for the whole set. The same procedure must be carried-out for rotations.

Then one must enter into the first data row the appropriate formulas, for each energy term through the equations (2), (3), (4), and propagate the calculation for the entire columns, and finally one may use the calculated values to build the various graphs.

A much easier and faster method may be the dynamical modeling], as shown later.

## VII. DYNAMICAL MODELING

In the previous section we used Excel to obtain a first look at the energy analysis (figures 6, 7, 8) but this quite tedious process does not provide results entirely satisfactory. Some simulations of Wilberforce pendulum may be found on the web, however they do not offer the possibility to compare the results with experimental data nor do they usually present



an analysis of the energy aspects. [19,20,21]. Better suited for this purpose are today's readily available tools of *dynamical modeling*, which allow models to be built selecting and combining a few basic structural elements. Among the various possibilities, below we present results obtained with the free-software InsightMaker [22], which only requires an internet connection.

In InsightMaker we create the model using: a) "*reservoirs*" which represents physical quantities (extensive quantities that we can imagine to be "stored" in the system, as

momentum  $p=mv$ , angular momentum  $L=I\omega$ ; in figure 9 they are shown as rectangles; b) "*flow rates*", shown as thick segments with double-arrows, which implement, at each instant, the correct value of the incoming and/or outgoing exchanges of the reservoir to which they are connected; c) "*constants or variables*", shown as circles, which represent general physical quantities; d) "*links*", shown as lines with single-arrow (the arrow direction indicates which *primitive* affects the other *primitive*). A fifth primitive, named "*converter*", represented by a hexagon, allows a comparison between model results and experimental data imported as a CSV file.

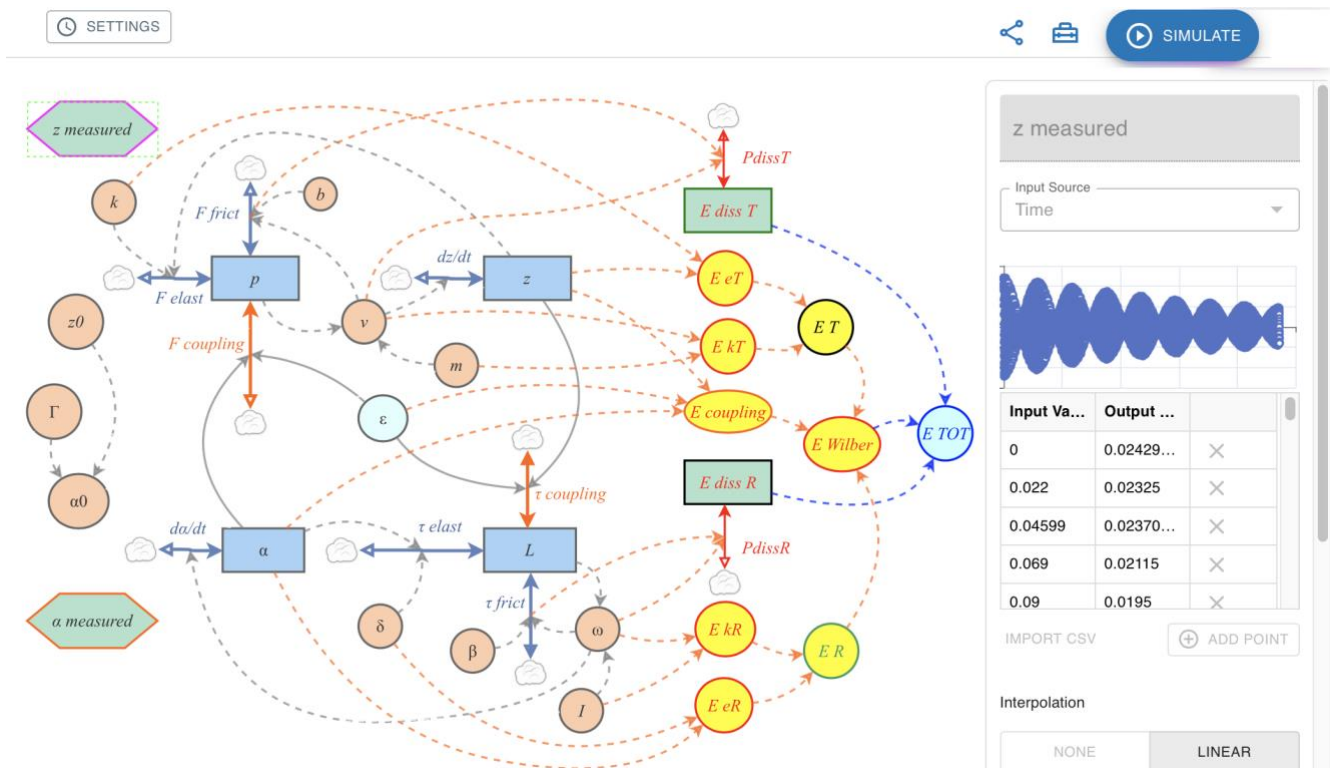


**FIGURE 9.** Dynamical model obtained with InsightMaker. The attached experimental data for translations may be seen by clicking on the primitive "z measured". The button "SIMULATE" starts the process and displays the graphs.

Our model was built as follows:

- for translational motion we define a *reservoir* for linear momentum  $p$ , connected to three different *flowrates*: one describing the exchanges due to the restoring elastic force  $F_{elastic} = -kz$ , one describing the exchanges due to the dissipative force (we choose a linear regime  $F_{frict} = -bv$  since the dissipation is due essentially to air friction), and finally one accounting for the coupling force  $F_{coupling} = -\varepsilon \alpha/2$ ;
- for rotational motion we define a *reservoir* for angular momentum  $L$ , with three *flowrates* one describing the restoring elastic torque  $\tau_{elastic} = -\delta\alpha$ , one describing the dissipative torque (for linear regime  $\tau_{frict} = -\beta\omega$ ), and one accounting for the coupling torque  $\tau_{coupling} = -\varepsilon z/2$ ;
- then we define a set of *variables* with constant values, representing all the parameters that characterize the

pendulum (the coefficients  $b$  and  $\beta$  must be properly chosen to fit the experimental damping);

- then we define the two *variables* for the linear velocity  $v=p/m$  and the angular velocity  $\omega=L/I$ ; these, interpreted as a rate of change, yield the values of vertical displacement  $z(t)$  and angular displacement  $\alpha(t)$  which are represented as *reservoirs* (values obtained by integration).

In order to determine the motion of the pendulum, it is also necessary to specify the initial conditions: for example we may choose to release the pendulum from rest, displacing it vertically (i.e.  $z(0)=z_0$ ), but without any rotation (i.e.  $\alpha(0)=0$ ).

At this stage, the model is complete as far as we are interested in the kinematics and dynamics of the pendulum motion. Before proceeding to the comparison between the

experimental data and the model results, we briefly discuss how the energy aspects are implemented. They are collected in the right part of the model (Figure 9):

- the four terms (kinetic and elastic energy for translations and rotations) are defined as *variables*, since all the quantities necessary to obtain them are already present in the model: for translation  $E_T = E_{kT} + E_{eT} = (mv^2 + kz^2)/2$ , for rotations:  $E_R = E_{kR} + E_{eR} = (I\omega^2 + \delta\alpha^2)/2$ , and for the coupling energy:  $E_{coupling} = \epsilon\alpha z/2$ . Finally we define the *variable*  $E_{Wilber} = E_T + E_R + E_{coupling}$  that gives the total energy associated with the pendulum;
- a different approach is needed for the dissipated energy, since it can only be expressed as integration of the dissipated power. In the model this translates to the use of a *flowrate-reservoir* pair for each motion: the *flowrates* define the instantaneous dissipation rates ( $P_{dissR} = \omega\tau_{frict}$ , and  $P_{dissT} = vF_{frict}$ ) while the *reservoirs* ( $E_{dissR}$ , and  $E_{dissT}$ ) give the value of dissipated energy;
- finally we use again a *variable* to define the total energy of the system  $E = E_{Wilber} + E_{dissR} + E_{dissT}$ : its time evolution will tell us whether or not our model conforms to the principle of conservation of energy.

Once the model is built, one needs only to set the simulation time step (e.g. 0.01 s), the algorithm type (we choose 4<sup>th</sup> order Runge-Kutta) and the simulation length.

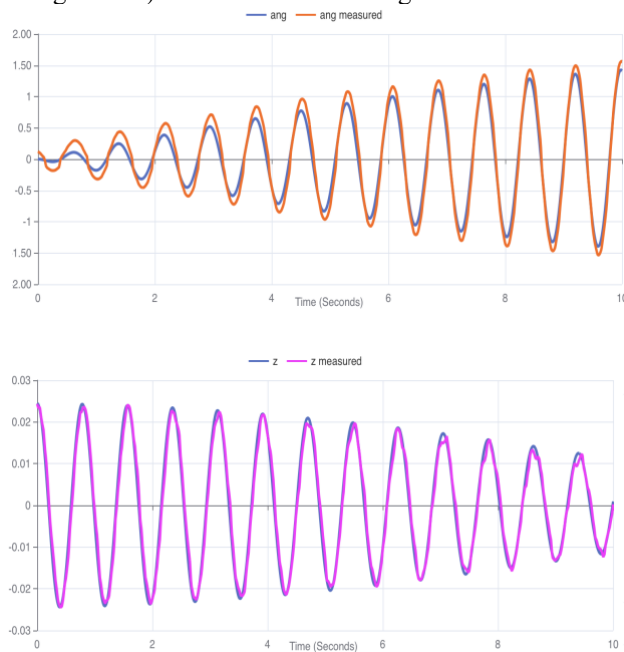


**FIGURE 10.** Comparison between experimental data (orange for displacement and violet for angle) and model results (blue).

First, we are interested in the comparison between model results and experimental data obtained for both vertical and torsional displacements: the overall trend (see figure 9, about 200 s) allows us to adjust the dissipation factors  $b$  and  $\beta$ . Figure 10 shows the detail of the first 10 seconds (where the blue line represents experimental data). The result can be rated as more than satisfactory.

In figure 11 we show the results for the evolution of the kinetic and elastic terms of translational motion, and in figure 12 the same for rotational motion.

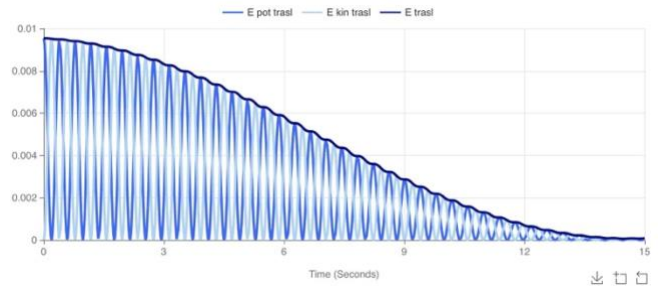


**FIGURE 11.** Energy evolution for the translational motion for 10 s.

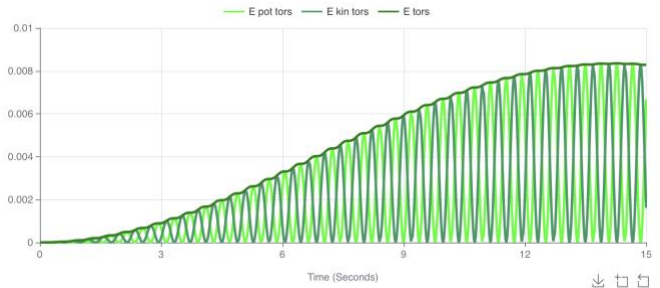


**FIGURE 12.** Energy evolution for the torsional motion for 10 s.

The time evolution of the various terms for much longer time is shown in figure 13: in particular we observe that the quantity  $E$  shows a constant value. This indicates that our model respects the energy principle.

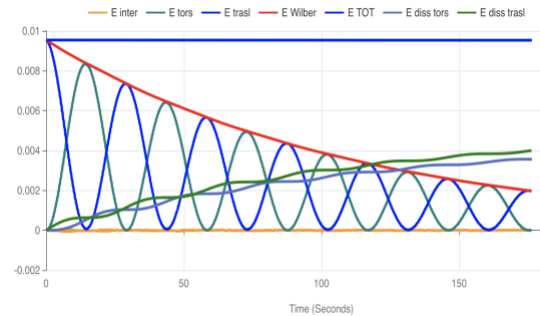


**FIGURE 13.** Energy graphs obtained with our model.

A close look at the graphs (figure 14) show that the *translation* dissipation-power (the slope of the corresponding curve) is maximum at  $t = 0$  s,  $t \approx 30$  s, ... (pure *translation*); the same occurs for the *torsional* dissipation-power at  $t \approx 15$  s,  $t \approx 45$  s, ... (pure *rotation*).

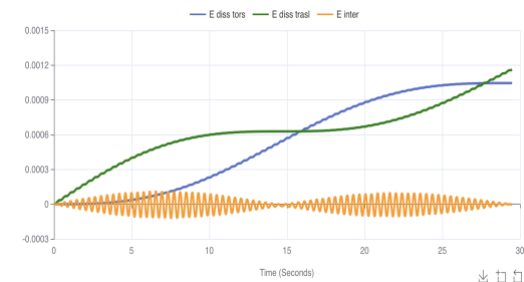


**FIGURE 14.** Details of the interaction energy and dissipated energies for the first 30 seconds.

The interaction energy oscillates with frequency  $2\omega$ , with a beating frequency  $2\omega_B$ , and reaches zero amplitude every time the motion is purely rotational or purely translational.

Finally, we illustrate the results for normal modes (figure 15).

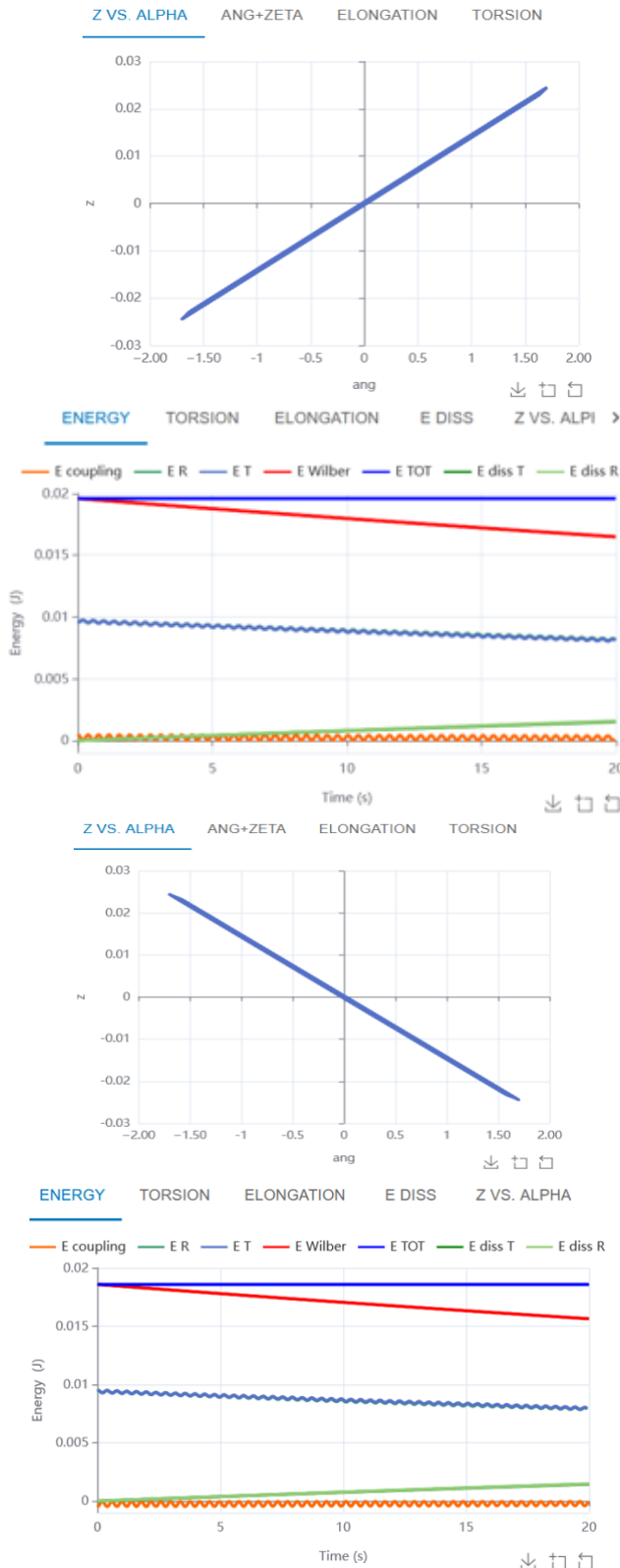


**Figure 15.** Normal modes: above, the trajectories in the  $z - \alpha$  plane, below the energy aspects. On top the results for normal mode 1 (oscillation in phase and higher energy), on bottom those for normal mode 2 (oscillation in phase opposition and lower energy) are shown.

These can be obtained by only changing the initial conditions values, which should be set (see Section V) as  $z_0 = +\Gamma\alpha_0$  for the normal mode 1 (in phase oscillation) and  $z_0 = -\Gamma\alpha_0$  for the normal mode 2 (oscillation in phase opposition).

Figure 15 shows also the energy aspects for the two normal modes: note that the interaction energy, while oscillating, is positive for the normal mode 1 and negative for the normal mode 2.

## VIII. CONCLUSIONS

The Wilberforce pendulum is a device that always arouses interest and curiosity [23] and is successfully used both in introductory and in advanced mechanics courses. It is particularly interesting from an educational point of view because it provides a nontrivial example of a system manifesting coupled oscillatory motions. There are also regular contributions on this subject in the literature, recently especially in relation to the use of new technologies (smartphone and video analysis systems [24]). In this paper we describe a novel apparatus that allows, using real time data acquisition, to independently capture both vertical and rotational displacement: using a MEMS driven by an EPS32 microcontroller with built-in WIFI and Bluetooth, in connection with the free *Phyphox* application it is possible to obtain data that *completely* characterize the motion.

The second part of the paper is devoted to analyzing the obtained data, particularly extending the analysis to energy aspects, first using the Excel spreadsheet, then making use of dynamic modeling. With the chosen software (*InsightMaker*), it was possible to highlight both the time evolution of the energy associated with the vertical and torsional oscillation motions, as well as that of the coupling energy and that of the dissipated energy, thus being able to verify the compatibility of the model with the principle of conservation of energy. By appropriately changing the initial conditions, to conclude we also obtained trajectories in 2-dimensional configuration space in the case of normal modes, an aspect that nicely highlights how the versatility of these tools is an example of an efficient didactical use of modern technologies.

## ACKNOWLEDGEMENTS

One of the authors (G. Torzo) thanks dr. Luca Bacci for the initial help in testing the MEMS sensor system.

## REFERENCES

- [1] Named after Robert Lionel Wilberforce, a physics demonstrator at the Cavendish Labs, who in 1894 showed how a cylindrical mass suspended to an helicoidal spring may undergo both rotational and longitudinal oscillations, later publishing a paper *On Vibrations of Loaded Spiral Spring*, on *Philosophical Magazine* **38**, 386 (1895)
- [2] U. Köpf, *Wilberforce's pendulum revisited*, *Am. J. Phys.* **58**, 833-837 (1990)
- [3] R. E. Berg and T. S. Marshall, *Wilberforce pendulum oscillations and normal modes*, *Am. J. Phys.* **59**, 32-38 (1991)
- [4] F. G. Karioris, *Wilberforce pendulum, demonstration size*, *The Phys. Teacher* **31**, 314-315 (1993)
- [5] M. Hübner and J. Kröger, *Adiabatic transfer in Wilberforce pendulum normal modes*, *Am. J. Phys.*, **86**, 818-824 (2018)
- [6] V. de Souza, P.G. Queiruga, E. Marinho Jr, *Experimental study of coupled oscillations on a Slinky Wilberforce*

pendulum, *Revista Brasileira de Ensino de Física*, **44**, e20220037(2022)

[7] A. Sommerfeld, *Lissajous-Figuren und Resonanzwirkungen bei schwingenden Schraubenfedern; ihre Verwertung zur Bestimmung des Poissonschen Verhältnisses*, in Adolph Wüllner Festschrift, Leipzig, 162-193 (1905)

[8] A. Sommerfeld, *Coupled oscillations of a helical spring*, *J. Optical Soc. A. Rev. Sci. Instr.*, **7**, 529-535 (1923)

[9] A. Sommerfeld, *Mechanics of deformable bodies: lectures on theoretical physics II*, Academic Press, New York, 308-314 (1950)

[10] E. Debowska, S. Jakubowicz, Z. Mazur: *Computer visualization of the beating of a Wilberforce pendulum*, *Eur. J. Phys.*, **20**, 89-95 (1999)

[11] P. Devaux, V. Piao Piau, O. Vignaud, G. Grosse, R. Olarte, and A. Nuttin, *Cross-camera tracking and frequency analysis of a cheap Slinky Wilberforce pendulum*, *Emergent Scientist* **3**, 1-8 (2019)

[12] B. Kos, M. Grodzicki and R. Wasielewski, *Electronic system for the complex measurement of a Wilberforce pendulum*, *Eur. J. Phys.* **39**, 1-6 (2018)

[13] M. H. Giménez, I. Salinas, J.A. Monsoriu, J. Castro-Palacio, *Direct Visualization of Mechanical Beats by Means of an Oscillating Smartphone*, *The Physics Teacher*, **55**, 424-425 (2017)

[14] L. F. Kasper, *New options for the old Wilberforce pendulum*, *The Phys. Teacher*, **61**, 628-629 (2023), and references therein

[15] J. Kuhn and P. Vogt, *Analyzing spring pendulum phenomena with a smart-phone acceleration sensor*, *The Phys. Teacher*, **50**, 504-505 (2012)

[16] For example: 3BScientific-U61021 and PASCO-ME8091

[17] It may be shown that gravitational potential energy may be excluded from the energy balance by an appropriate choice of the system and of the reference frame.

[18] T. Gallot, D. Gau, R. Garcia-Tejera, *Coupled oscillations of the Wilberforce pendulum unveiled by smartphones*, *Am. J. Phys.* **91**, 873-878 (2023)

[19] A.F. Garcia: *Interactive Physics Course on the Internet* <<http://www.sc.ehu.es/sbweb/fisica3/oscilaciones/wilberforce/wilberforce.html>> 2016

[20] *Wolfram Demonstration Project*, <<https://demonstrations.wolfram.com/TheWilberforcePendulum>>

[21] <<http://insightmaker.com/>>

[22] the model is freely accessible at <<https://insightmaker.com/insight/C5VBczd4ntwDOnzWp4vaO/LAJPE-energy-Wilberforce>>. A detailed description of the model construction as well as the complete list of equations can be requested to the authors.

[23] C. Ucke, H.J. Schlichting, *Das Vallet Federpendel*, *Phys. Unserer Zeit*, **4**, 197-199 (2021)

[24] Q. Wen and L. Yan, *Theoretical and experimental studies of the Wilberforce pendulum*, *Eur. J. Phys.* **42**, 1-25 (2021)